 E-ISSN: 2303-0720

DOI: https://doi.org/10.21009/JRSKT.121.03

Molecular Docking Insights into EDTA and Tween-20-Induced Inhibition of Lysozyme in Bacterial DNA Isolation Buffers

Ika Keumala Fitri[1*], Meredith Jannaatu 'Adn[1], Tegar Cahya Widodo[1], Muktiningsih Nurjayadi[1], Futi Kusuma Hati[1]

[1]*Chemistry Study Program, Faculty of Mathematics and Natural Sciences, Universitas Negeri Jakarta, Jl. Rawamangun Muka, Rawamangun, Jakarta Timur, DKI Jakarta 13220, Indonesia*

*Email: ikakeumala@unj.ac.id

Received: 30 November 2025
Revised: 01 May 2025
Accepted: 13 June 2026
Online: 24 June 2026
Published: 30 June 2026

Jurnal Riset Sains dan Kimia Terapan
p-ISSN: 2302 - 8467
e-ISSN: 2303 – 0720

Abstract

The efficiency of bacterial deoxyribonucleic acid (DNA) isolation is a critical bottleneck in Polymerase Chain Reaction (PCR) based pathogen detection. This study investigates the potential inhibitory effects of standard lysis buffer components, including ethylenediaminetetraacetic acid (EDTA), Tris base, and Tween-20, on Hen Egg White Lysozyme (HEWL) to address the low DNA yields observed in a locally developed isolation kit. Molecular docking simulations were performed using AutoDock 4.2.6. The protocol was validated by redocking the native ligand, which established the suitability of a 60x60x60 Å grid box. The results revealed that EDTA binds with high affinity, with an intermolecular energy of -6.44 kcal/mol, and interacts with crucial anchoring residues Trp62 and Asp101. Notably, the hydrophobic tail of Tween-20 exhibited the strongest binding (-7.12 kcal/mol), penetrating the active cleft and blocking the catalytic residue Glu35. Conversely, Tris base and the hydrophilic head of Tween-20 showed weaker, less stable interactions. These findings suggest a dual-inhibition mechanism in which EDTA blocks substrate access, while Tween-20 hinders the catalytic center. This study provides a molecular explanation for the kit's reduced performance and highlights the need for buffer optimization.

Keywords: Enzyme Inhibition, DNA Isolation, Lysozyme, Molecular Docking.

Introduction

High-quality and pure genomic DNA isolation is a crucial step in various molecular biology applications, such as PCR (Polymerase Chain Reaction), sequencing, and cloning. The integrity of the isolated template is a fundamental determinant of PCR efficiency and downstream diagnostic reliability (Kralik & Ricchi, 2017). The research group PUI (*Pusat Unggulan IPTEK*) Pendeteksi Bakteri Patogen Universitas Negeri Jakarta focused on developing a foodborne pathogen detection kit targeting specific genes using PCR (Nurjayadi et al., 2025). The need for such kits becomes more significant with the rising global and local foodborne outbreaks, which require rapid PCR optimizations to detect critical

 E-ISSN: 2303-0720

pathogens such as *Vibrio parahaemolyticus* (Nurjayadi et al., 2025) and other zoonotic agents (Chlebicz & Śliżewska, 2018). This kit is a potentially crucial tool for Indonesia's MBG (Makan Bergizi Gratis) program, especially for monitoring food safety. Ensuring the absence of pathogens in processed food products, such as fermented milk and other high-protein derivatives, is vital for consumer health (Purwani & Kartika, 2019) and for preventing widespread public health incidents associated with microbial contamination in food supply chains (Bintsis, 2017).

To improve the kit's economic efficiency, the research intends to develop a reliable bacterial DNA isolation kit. After all, the detection of pathogenic bacteria, such as *Pseudomonas aeruginosa*, which causes various infections, relies heavily on the efficient extraction of genetic material from bacterial cells (Hati et al., 2025). These efficient extraction methods are paramount when handling the robust membrane cells of Gram-positive pathogens, such as *Staphylococcus aureus* (Juliandoz et al., 2025), whose thick, cross-linked peptidoglycan architecture and dense surface porosity pose significant challenges for standard lysis protocols (Pasquina-Lemonche et al., 2020).

This kit was initially built using the group's standardized Standard Operating Procedure (SOP), which used a lysis buffer containing TE (Tris-EDTA/ethylenediaminetetraacetic acid) and Tween-20 (polysorbate) at pH 8. However, significant challenges arose: the isolated DNA was of poor quality, with smeared or absent bands in agarose gel electrophoresis. Smeared bands typically indicate DNA shearing or nuclease-mediated degradation due to incomplete cell lysis (Na et al., 2025). This also indicates a failure in the purification process, preventing proper DNA migration, a common bottleneck in molecular diagnostics (Li et al., 2020).

Bacterial lysis relies heavily on the efficacy of lysozyme, an enzyme capable of hydrolyzing the β-(1,4) link between N-acetylmuramate and N-acetylglucosamine (peptidoglycan) in the cell wall (Naveed et al., 2023). The proper structural configuration of lysozyme is essential for its optimal anti-bacterial activities (Ragland & Criss, 2017). HEWL, commonly used in laboratories, features a deep, cleft-like active site whose structural conformation is critical for substrate binding (Nam, 2025). This active site is divided into subsites A-F, which bind specific sugar residues (Zeng et al., 2021). The catalytic mechanism relies on precise interactions between these subsites (**Figure 1**, **Table 1**). At the cleft entrance (Subsites A-B), Asp101 and Asn103 act as initial anchors for the sugar rings (Nam, 2025). Deeper in the cleft at Subsite C, Trp62 and Trp63 provide essential hydrophobic anchoring (Das et al., 2018), while Asn59 and Ala107 enforce substrate specificity by bonding with the N-acetyl group (Ogata et al., 2021). The structural integrity and hydrophobic pockets required for the reaction are maintained by Ile58, Val109, and Trp108 (Zeng et al., 2021), the latter being crucial for maintaining the protonation state of Glu35 (Singh et al., 2022). Finally, Gln57 positions of the scissile bond, allowing Glu35 and Asp52 to facilitate the cleavage of the glycosidic bond between subsites D and E (Naveed et al., 2023; Singh et al., 2022).

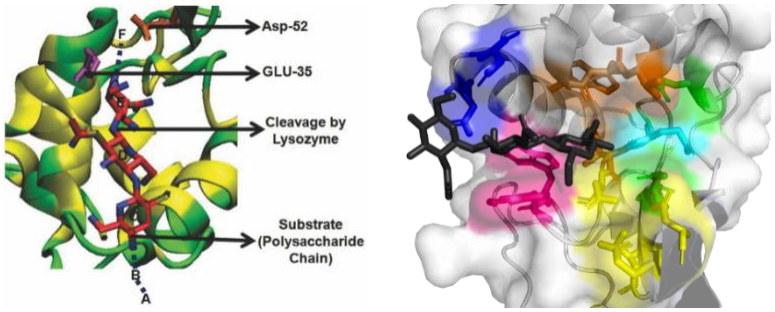

(A) (B)

Figure 1. HEWL binds to NAG3, with its (A) subsite locations (Roy et al., 2012) and (B) the locations of several crucial amino acid residues visualized with VMD, as shown in **Table 1**.

However, the accessibility of HEWL's active site can be a disadvantage: it allows small molecules or structural mimics to bind and inhibit enzymatic activity. Research has shown that various compounds, including transition-state analogues and flavonoids such as naringin, can bind tightly to the active site via hydrogen bonding and hydrophobic interactions, effectively blocking the native substrate (Das et al., 2018; Ogata et al., 2021). Consequently, to address the failure of the DNA

 E-ISSN: 2303-0720

isolation procedure, it is imperative to investigate whether the buffer components, Tris base, EDTA, and Tween-20, act as unintended inhibitors.

Table 1. Key residues of HEWL (Das et al., 2018; Nam, 2025; Naveed et al., 2023; Ogata et al., 2021; Singh et al., 2022; Zeng et al., 2021)

Subsite	Key Residues	Color	Primary Role	Interaction Mechanism (for reference)
A-B	Asp101	Blue	Entry anchor, binds sugar rings	Hydrogen bond
A-B	Asn103	Blue	Surface binding	Hydrogen bond
C	Asn59	Yellow	Hydrogen bonding network	Hydrogen bond
C	Trp62	Pink	Substrate binding	Hydrophobic / Stacking
C	Trp63	Pink	Substrate binding	Hydrophobic / Hydrogen bond
C	Ile58	Orange	Binding/stability	Hydrophobic
C	Ala107	Orange	Specificity	Hydrogen bond
D	Trp108	Orange	Structural/environment	Hydrophobic
D	Val109	Orange	Steric fit	Hydrophobic
D-E	Glu35	Green	Catalytic (Acid/base)	Acts as a general acid catalyst
D-E	Asp52	Green	Catalytic (stabilizer)	Electrostatic
E	Gln57	Cyan	Cleavage site positioning	Hydrogen bond

EDTA, a chelating agent, may inhibit HEWL by altering the electrostatic environment or stripping metal ions that, while not always catalytic, can influence enzyme stability and activity (Sullivan et al., 2017). Meanwhile, Tween-20 could potentially interfere with HEWL's native conformation or protein-protein interactions, similar to how other amphiphilic molecules modulate lysozyme structure (Chaari et al., 2019). Despite their use in various fields for buffer composition, we found no structural or computational evidence investigating whether these reagents affect lysozyme in a manner similar to a competitive inhibitor by binding directly to HEWL's binding site.

To address this gap, this research presents a novel approach that employs molecular docking as an in-silico method to investigate the binding affinities and interaction modes of EDTA, Tris base, and Tween-20 with the HEWL active site. This method has been proven reliable for screening bioactivity and molecular binding affinities at the atomic level (Prasetiyo et al., 2025). This study aims to identify potential inhibitory interactions that may compromise the PUI research group's DNA isolation kit and to conduct the first in silico study to evaluate standard buffer compositions as potential inhibitors of HEWL.

Method

Ligand and Protein Preparation.

The crystal structure of HEWL was retrieved from the RCSB Protein Data Bank (PDB) (Burley et al., 2021) under the accession code 1HEW (Diamond, 1974). The native ligand, tri-N-acetyl-D-glucosamine (NAG3), was extracted from the 1HEW PDB file for validation. NAG3 was chosen as the native ligand because it is the substrate analogue of peptidoglycan, lysozyme's natural substrate. Because of their structural similarity, NAG3 acts as a competitive inhibitor of lysozyme with strong binding (Ogata et al., 2021). Hydrogen atoms were added to the NAG3 structure using Avogadro 1.2.0 (Hanwell et al., 2012) to ensure valency and calculation accuracy.

For the experimental ligands, comprising EDTA, Tris base, and Tween-20, structures were prepared and protonated to simulate a pH 8.0 environment using Avogadro, reflecting the conditions of the DNA isolation buffer (Singh et al., 2022). Due to the large size and high flexibility of Tween-20, which pose a challenge for standard docking algorithms, the molecule was fragmented into two functional moieties: the hydrophilic head (Tween-head) and the hydrophobic tail (Tween-tail) (Forli et al., 2016).

 E-ISSN: 2303-0720

Molecular Docking Protocol.

All molecular docking simulations, preparations, and visualizations were performed on a Lenovo IdeaPad Slim 5 14IMH9 running Windows 11 Home Single Language (64-bit), equipped with Intel® Arc™ Graphics and 16.0 GB of RAM. Docking simulations were performed using AutoDock 4.2.6 following the standard protocol for rigid-receptor docking (Forli et al., 2016). First, redocking validation was conducted using NAG3 to optimize the search space. Three Grid Box dimensions were evaluated: 50x50x50 Å (50-box), 60x60x60 Å (60-box), and 70x70x70 Å (70-box), and each simulation was done three times. These box sizes were chosen because of the enormous size of several compounds used, such as Tween-20, making a 40x40x40 Å box out of the question. The Lamarckian Genetic Algorithm (LGA) was set to 50 runs for the validation step to ensure convergence in conformational sampling (Pinzi & Rastelli, 2019). The parameter used will be the average from all three simulations of each box.

Following validation, the grid box configuration that yielded the lowest Root Mean Square Deviation (RMSD) (< 2.0 Å) relative to the crystal structure was selected for the target ligands, in accordance with standard validation metrics (Ramírez & Caballero, 2018). EDTA, Tris base, Tween-head, and Tween-tail were docked into the HEWL active site using 100 LGA runs, and each simulation was repeated 3 times. This increased run count was used to maximize the probability of identifying the global minimum-energy conformation and to map potential binding sites across the enzyme surface. The parameter used will be the average from all three simulations of each compound.

Analysis and Visualization.

The resulting conformations were ranked by their lowest binding energy (ΔG). Post-docking analysis and visualization were performed in PyMOL 3.1.1 (Schrödinger, 2021) to assess structural poses and identify key residues. Detailed characterization of non-covalent interactions (hydrogen bonds, hydrophobic contacts, and π-stacking) was performed using LigPlus 2.3 (Laskowski & Swindells, 2011).

Result and Discussion

Validation of Molecular Docking Protocol.

The docking protocol was validated by redocking the native ligand, NAG3, a competitive inhibitor and substrate analogue of lysozyme (Ogata et al., 2021). Given the deep cleft architecture of the HEWL active site (Nam, 2025), optimizing the grid box size is critical to ensure adequate conformational sampling. We evaluated three grid box dimensions (50-box, 60-box, and 70-box) with triplicate analyses to determine the minimum size required to encompass the active site and the large surfactant ligands. Proper grid box scaling is essential in rigid-receptor docking, as an excessively large box can result in false positives and reduce the efficiency of the conformational search algorithm (Forli et al., 2016).

As presented in **Table 2**, the redocking results demonstrated acceptable accuracy. While the 50-box yielded an RMSD of 1.90 Å and satisfied the standard threshold of RMSD ≤ 2.0 Å (Ramírez & Caballero, 2018), the larger boxes (60-box and 70-box) produced RMSD values of 2.14 Å and 2.06 Å, respectively. These values are acceptable for large, flexible ligands like carbohydrates, indicating that the redocked ligand occupies the same binding pocket as the crystallographic reference (Pinzi & Rastelli, 2019). This redocking procedure is a gold-standard preliminary step for verifying that the chosen docking algorithms and grid parameters reliably reproduce known experimental binding poses before proceeding to novel targets (Lee et al., 2025).

Table 2. Results of NAG3 redocking

Box Size (Å)	RMSD (Å)	Cluster Size	Intermolecular Energy (kcal/mol)	Total Binding Energy (kcal/mol)
50x50x50	1.9	2	-8.26	-2.89
60x60x60	2.14	3	-6.15	-0.78
70x70x70	2.06	2	-5.15	0.22

 E-ISSN: 2303-0720

This structural fidelity is further confirmed by the interaction analysis, which is completely retained throughout the three simulations for each box size (**Table 3**). The redocked NAG3 retained critical hydrogen bonds with Asn59, Trp62, Trp63, and Ala107, mirroring the native structure. Different interactions, such as the loss of interaction with Gln57 and the formation of new hydrophobic contact with Ile58, are attributed to slight conformational shifts allowed within the docking algorithm to minimize internal strain (Nam, 2025). Such subtle repositioning is commonly observed in flexible-ligand simulations within the highly dynamic cleft of HEWL, reflecting the natural plasticity of the protein-ligand interface (Ali et al., 2024).

Table 3. Protein-ligand interactions of HEWL and NAG3

Key Residues	Interaction (Reference)	Formed interactions between NAG3 and the amino acid residue			
		Original	50x50x50 Å	60x60x60 Å	70x70x70 Å
Asp101	Hydrogen bond	V	V	V	V
Asn103	Hydrogen bond	V	V	-	V
Asn59	Hydrogen bond	V	V	V	V (H)
Trp62	Hydrophobic	V (HB)	V (HB)	V	V (HB)
Trp63	Hydrogen bond/Hydrophobic	V (HB)	V (HB)	V (HB)	V (H)
Ile58	Hydrophobic	-	V	V	-
Ala107	Hydrogen bond	V	V	V	V
Trp108	Hydrophobic	V	V	V	-
Gln57	Hydrogen bond	V (H)	-	V (H)	-

Several annotated checklists have different interactions from the reference, with HB: Hydrogen bond, and H: Hydrophobic.

The energetic analysis (**Table 2**) revealed lower negative total binding energies for NAG3, a typical AutoDock 4 case for ligands with many rotatable bonds, due to high torsional penalty scores (Forli et al., 2016). The Autodock's empirical scoring function specifically penalizes highly flexible molecules to account for the freezing of rotatable bonds upon binding, which can sometimes skew the total binding energy relative to more rigid molecules (Eberhardt et al., 2021). However, the intermolecular energy, which represents the direct affinity between the ligand and protein, was strongly negative (-6.15 to -8.26 kcal/mol), consistent with theoretical expectations for stable binding (Forli et al., 2016). Consequently, intermolecular energy will be used as the primary metric for comparing the target ligands, rather than total binding energy. Ultimately, the 60-box was selected for subsequent docking to accommodate the large spatial requirements of Tween-20 while maintaining computational efficiency and interaction accuracy.

Binding Mode of Target Ligands.

Unlike NAG3, which spans subsites C-E (Ogata et al., 2021), Tris base and EDTA are smaller molecules, resulting in distinct binding profiles (**Table 4**). EDTA exhibited two dominant binding clusters. Cluster 1 occupied the solvent-exposed region near subsites A and B (**Figure 2A**) with high consistency, as evidenced by its large cluster size (70 conformations out of 100 runs). Although spatially distinct from the deep catalytic center, unlike the Cluster 6 conformation (**Figure 2B**), this cluster demonstrated a high intermolecular energy of -6.44 kcal/mol, surpassing that of the redocked NAG3 in the 60-box. Crucially, EDTA in Cluster 1 interacts with Trp62 and Asp101 (**Figure 3A**, **Table 5**). Since Trp62 is essential for anchoring the substrate via hydrophobic stacking (Das et al., 2018) and Asp101 stabilizes the substrate at the entry cleft, EDTA binding at this location suggests a potential blockage of substrate entry. Because a deep catalytic site is often accessible only through narrow entryways, small chelators or inhibitors binding at these peripheral sites can cause steric occlusion, effectively preventing native substrates from reaching the core catalytic residues (Guedes et al., 2014).

Next, the surfactant component, Tween-20, is analyzed. The amphiphilic nature of Tween-20 necessitated the separate docking of its hydrophilic head and hydrophobic tail. Nevertheless, it turned

 E-ISSN: 2303-0720

out that the Tween head still presented challenges in the 60-box, yielding a singular, non-clustered conformation (Cluster size: 1) due to steric clashes within the cleft (**Table 4**). This is also evident from the twisted 3D structure of the Tween head after docking (**Figure 4**). Expanding the grid to 70x70x70 Å improved the clustering (Cluster size: 30) and its 3D structure (**Figure 4**), indicating that the smaller box restricted the conformational freedom of the bulky head group. However, even in the optimal box, the intermolecular energy remained moderate (-4.83 kcal/mol) even though the Tween head binds onto several important residues of HEWL, suggesting that the hydrophilic head group of Tween-20 alone does not drive potent inhibition. Surfactant head groups, particularly bulky non-ionic polyoxyethylene chains similar to those in Tween-20, often exhibit severe steric hindrance and hydration-shell conflicts that can also prevent their penetration into the deep, narrow enzyme clefts (Otzen, 2011).

Table 4. Docking results of all target ligands in HEWL

Ligand Name	Grid box type	Cluster Size	Intermolecular Energy (kcal/mol)	Total Binding Energy (kcal/mol)
EDTA (Cluster 1)	60-box	70	-6.44	-3.16
EDTA (Cluster 6)	60-box	6	-4.73	-1.45
Tris	60-box	30	-4.83	-2.74
Tween head	60-box	1	-6.44	-3.16
Tween head	70-box	30	-4.83	-2.74
Tween tail	60-box	34	-7.12	-3.54

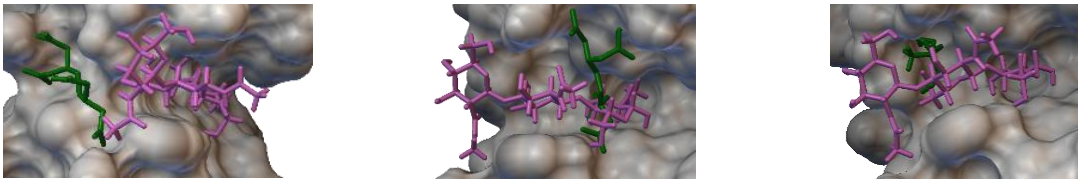

(A) (B) (C)

Figure 2. The location of (A) EDTA Cluster 1, (B) EDTA Cluster 6, and (C) Tris (each target ligand in green) compared to the original NAG3 (in pink).

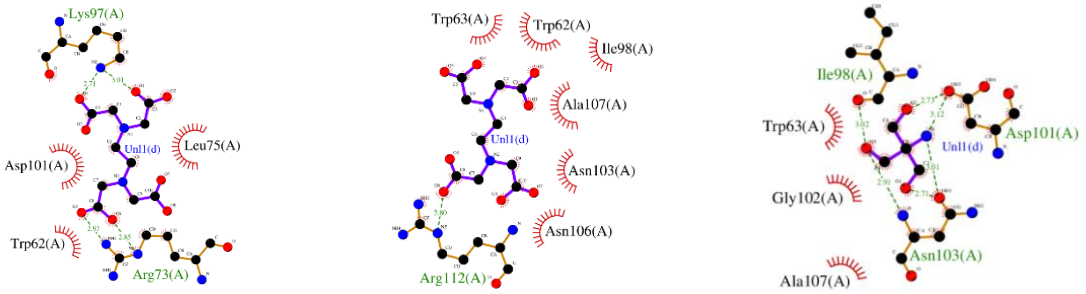

(A) (B) (C)

Figure 3. The schematic of protein-ligand interactions between HEWL and (A) EDTA Cluster 1, (B) EDTA Cluster 6, and (C) Tris

In contrast, the Tween tail (hydrophobic chain) did not have the same problem as the Tween head and even demonstrated significantly stronger binding. Using the 60-box, the tail yielded an intermolecular energy of -7.12 kcal/mol, which is stronger than the redocked NAG3 (**Table 4**). The tail formed extensive hydrophobic interactions, surpassing the number of contacts observed for EDTA, Tris, or Tween head (**Table 5**, **Figure 5**). This behavior aligns with the tendency of hydrophobic chains to bury themselves within the apolar regions of the active site cleft to minimize solvent exposure (Zeng et al., 2021). Experimental and computational analyses of protein-surfactant interactions consistently

 E-ISSN: 2303-0720

demonstrate that long, flexible hydrophobic tails are the core cause of strong, competitive binding within apolar enzymatic cavities, often leading to inhibition (Javadi et al., 2022).

Table 5. Protein-ligand interactions of HEWL and target ligands

Key Residues	Interaction (Reference)	Formed interactions between the target ligands and the amino acid residue					
		EDTA (Cluster 1)	EDTA (Cluster 6)	Tris	Tween head (60-box)	Tween head (70-box)	Tween tail
Asp101	Hydrogen bond	V (H)	-	V	V (H)	V (H)	V (H)
Asn103	Hydrogen bond	-	V	V	-	-	V
Asn59	Hydrogen bond	-	-	-	V	-	-
Trp62	Hydrophobic	V	V	-	V (HB)	V (HB)	-
Trp63	Hydrogen bond/Hydrophobic	-	V (H)	V (H)	V (HB)	V (HB)	V (H)
Ile58	Hydrophobic	-	-	-	V	V	-
Ala107	Hydrogen bond	-	V (H)	V (H)	V	V (H)	V (H)
Trp108	Hydrophobic	-	-	-	V	V	V
Glu35	Acid catalyst	-	-	-	-	-	V (H)
Asp52	Electrostatic	-	-	-	V	-	-
Gln57	Hydrogen bond	-	-	-	V	-	V (H)

Several annotated checklists have different interactions from the reference, with HB: Hydrogen bond, and H: Hydrophobic.

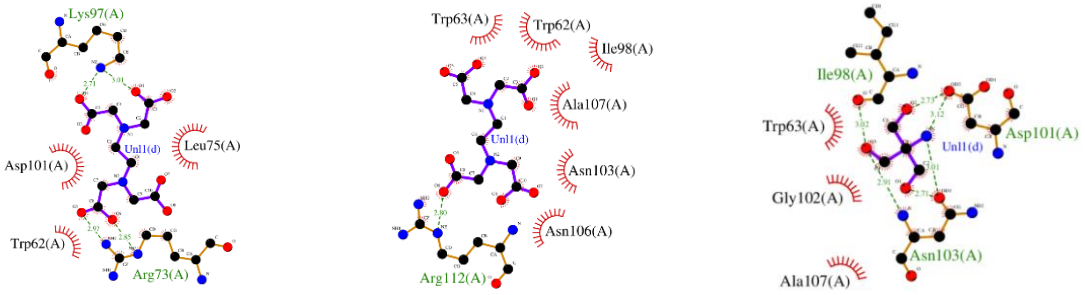

(A) (B) (C)

Figure 4. The schematic of protein-ligand interactions between HEWL and (A) EDTA Cluster 1, (B) EDTA Cluster 6, and (C) Tris

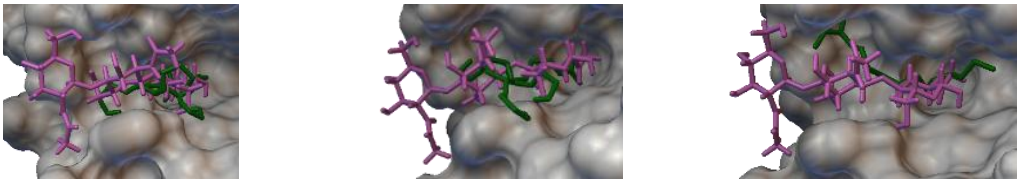

(A) (B) (C)

Figure 5. The location of (A) Tween head 60-box, (B) Tween head 70-box, and (C) Tween tail (target ligands in green) compared to the original NAG3 (in pink).

Based on the docking results, the hydrophobic chain of Tween-20 presents a direct threat to catalytic function. Notably, it interacts with Glu35, the general acid catalyst essential for glycosidic bond cleavage (Naveed et al., 2023; Singh et al., 2022). By occupying the hydrophobic pocket required

 E-ISSN: 2303-0720

for Glu35's correct protonation state, the surfactant tail could effectively silence the enzyme's catalytic machinery. These *in silico* findings indicate that standard DNA isolation buffers containing high concentrations of EDTA and Tween-20 may inadvertently reduce lysozyme efficiency, warranting further experimental optimization or protocol adjustment.

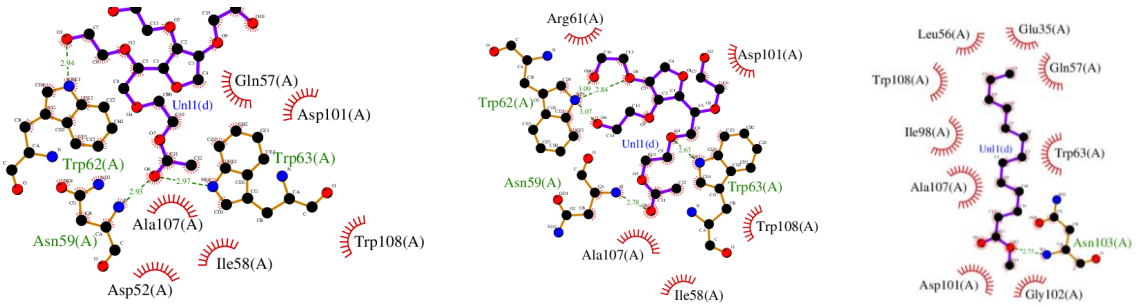

(A) (B) (C)

Figure 6. The schematic of protein-ligand interactions between HEWL and (A) Tween head (60-box), (B) Tween head (70-box), and (C) Tween tail

Conclusion

This study successfully evaluated the interaction of standard DNA isolation reagents with the active site of Hen Egg White Lysozyme (HEWL) using molecular docking. The findings indicate that EDTA and Tween-20 possess significant potential to act as competitive inhibitors, which correlates with the suboptimal DNA yields observed in the laboratory. Specifically, EDTA forms stable complexes at the entrance of the active site (Subsites A-C), interacting with Trp62 and Asp101, potentially acting as a steric barrier to the peptidoglycan substrate. Furthermore, the hydrophobic tail of Tween-20 has a strong tendency to bury itself within the catalytic cleft, directly blocking Glu35, the general-acid catalyst essential for cell wall hydrolysis. In contrast, Tris base and the Tween-20 head group exhibited weaker affinities and are less likely to be primary inhibitors. Based on these *in silico* results, we recommend optimizing the lysis buffer formulation, specifically by reducing the Tween-20 concentration or modifying the EDTA addition sequence to restore lysozyme efficiency and improve the sensitivity of the bacterial pathogen detection kit.

Reference

Ali, M. S., Al-Lohedan, H. A., Bhati, R., & Muthukumaran, J. (2024). Interaction of the lysozyme with anticoagulant drug warfarin: Spectroscopic and computational analyses. *Heliyon*, *10*(10), e30818. https://doi.org/10.1016/J.HELIYON.2024.E30818

Bintsis, T. (2017). Foodborne pathogens. *AIMS Microbiology 2017 3:529*, *3*(3), 529–563. https://doi.org/10.3934/MICROBIOL.2017.3.529

Burley, S. K., Bhikadiya, C., Bi, C., Bittrich, S., Chen, L., Crichlow, G. V., Christie, C. H., Dalenberg, K., Di Costanzo, L., Duarte, J. M., Dutta, S., Feng, Z., Ganesan, S., Goodsell, D. S., Ghosh, S., Green, R. K., Guranovic, V., Guzenko, D., Hudson, B. P., … Zhuravleva, M. (2021). RCSB Protein Data Bank: powerful new tools for exploring 3D structures of biological macromolecules for basic and applied research and education in fundamental biology, biomedicine, biotechnology, bioengineering and energy sciences. *Nucleic Acids Research*, *49*(D1), D437–D451. https://doi.org/10.1093/NAR/GKAA1038

Chaari, A., Fahy, C., Chevillot-Biraud, A., & Rholam, M. (2019). Investigating the effects of different natural molecules on the structure and oligomerization propensity of hen egg-white lysozyme. *International Journal of Biological Macromolecules*, *134*, 189–201. https://doi.org/10.1016/J.IJBIOMAC.2019.05.048

 E-ISSN: 2303-0720

Chlebicz, A., & Śliżewska, K. (2018). Campylobacteriosis, Salmonellosis, Yersiniosis, and Listeriosis as Zoonotic Foodborne Diseases: A Review. *International Journal of Environmental Research and Public Health 2018, Vol. 15, Page 863*, *15*(5), 863. https://doi.org/10.3390/IJERPH15050863

Das, S., Ghosh, P., Koley, S., & Singha Roy, A. (2018). Binding of naringin and naringenin with hen egg white lysozyme: A spectroscopic investigation and molecular docking study. *Spectrochimica Acta Part A: Molecular and Biomolecular Spectroscopy*, *192*, 211–221. https://doi.org/10.1016/J.SAA.2017.11.015

Diamond, R. (1974). Real-space refinement of the structure of hen egg-white lysozyme. *Journal of Molecular Biology*, *82*(3), 371–391. https://doi.org/10.1016/0022-2836(74)90598-1

Eberhardt, J., Santos-Martins, D., Tillack, A. F., & Forli, S. (2021). AutoDock Vina 1.2.0: New Docking Methods, Expanded Force Field, and Python Bindings. *Journal of Chemical Information and Modeling*, *61*(8), 3891–3898. https://doi.org/10.1021/ACS.JCIM.1C00203

Forli, S., Huey, R., Pique, M. E., Sanner, M. F., Goodsell, D. S., & Olson, A. J. (2016). Computational protein–ligand docking and virtual drug screening with the AutoDock suite. *Nature Protocols 2016 11:5*, *11*(5), 905–919. https://doi.org/10.1038/nprot.2016.051

Guedes, I. A., de Magalhães, C. S., & Dardenne, L. E. (2014). Receptor-ligand molecular docking. *Biophysical Reviews*, *6*(1), 75–87. https://doi.org/10.1007/S12551-013-0130-2

Hanwell, M. D., Curtis, D. E., Lonie, D. C., Vandermeerschd, T., Zurek, E., & Hutchison, G. R. (2012). Avogadro: an advanced semantic chemical editor, visualization, and analysis platform. *Journal of Cheminformatics 2012 4:1*, *4*(1), 17-. https://doi.org/10.1186/1758-2946-4-17

Hati, F. K., Rismaya, R., & Aurellia, D. G. (2025). In Vitro Evaluation of the Antibacterial Effect of Virgin Coconut Oil Against Pseudomonas aeruginosa Associated with Folliculitis. *Jurnal Riset Sains Dan Kimia Terapan*, *11*(1), 40–46. https://doi.org/10.21009/JRSKT.111.05

Javadi, A., Dowlati, S., Shourni, S., Miller, R., Kraume, M., Kopka, K., & Eckert, K. (2022). Experimental techniques to study protein–surfactant interactions: New insights into competitive adsorptions via drop subphase and interface exchange. *Advances in Colloid and Interface Science*, *301*, 102601. https://doi.org/10.1016/J.CIS.2022.102601

Juliandoz, Dzulhijar, Ningrum, S. A., Situmeang, B., Yulianti, N., Bilangi, N., Musa, W. J. A., & Rondonuwu, M. (2025). Potential of the Ethyl Acetate Extract of Kesambi (Schleichera oleosa) Bark as an Ointment-Based Treatment for Skin Diseases Against Staphylococcus aureus. *Jurnal Riset Sains Dan Kimia Terapan*, *11*(2), 23–30. https://doi.org/10.21009/JRSKT.112.03

Kralik, P., & Ricchi, M. (2017). A basic guide to real time PCR in microbial diagnostics: Definitions, parameters, and everything. *Frontiers in Microbiology*, *8*(FEB), 239909. https://doi.org/10.3389/FMICB.2017.00108

Laskowski, R. A., & Swindells, M. B. (2011). LigPlot+: Multiple Ligand–Protein Interaction Diagrams for Drug Discovery. *Journal of Chemical Information and Modeling*, *51*(10), 2778–2786. https://doi.org/10.1021/CI200227U

Lee, J., Hao Nguyen, C., & Mamitsuka, H. (2025). Beyond rigid docking: deep learning approaches for fully flexible protein–ligand interactions. *Briefings in Bioinformatics*, *26*(5). https://doi.org/10.1093/BIB/BBAF454

Li, X., Bosch-Tijhof, C. J., Wei, X., de Soet, J. J., Crielaard, W., Loveren, C. van, & Deng, D. M. (2020). Efficiency of chemical versus mechanical disruption methods of DNA extraction for the identification of oral Gram-positive and Gram-negative bacteria. *Journal of International Medical Research*, *48*(5). https://doi.org/10.1177/0300060520925594

Na, B., Park, J., Park, S., Park, E., Jang, J., Kim, Y. H., Lee, J., & Chung, H. S. (2025). Comparison evaluation of bacterial DNA extraction methods for improved molecular diagnostic accuracy of sepsis-causing pathogens in clinical whole blood samples. *Scientific Reports 2025 15:1*, *15*(1), 4167-. https://doi.org/10.1038/s41598-025-87225-y

Nam, K. H. (2025). Temperature-Dependent Structural Changes of the Active Site and Substrate-Binding Cleft in Hen Egg White Lysozyme. *Crystals*, *15*(2), 111. https://doi.org/10.3390/CRYST15020111

Naveed, M., Wang, Y., Yin, X., Chan, M. W. H., Aslam, S., Wang, F., Xu, B., & Ullah, A. (2023). Purification, Characterization and Bactericidal Action of Lysozyme, Isolated from Bacillus subtillis BSN314: A Disintegrating Effect of Lysozyme on Gram-Positive and Gram-Negative

 E-ISSN: 2303-0720

Bacteria. *Molecules*, *28*(3), 1058. https://doi.org/10.3390/MOLECULES28031058

Nurjayadi, M., Krisdawati, I., Declan, J. L., Putri, G. I., Juliansyah, D. A., Rahmawati, A. N., Fitriyanti, A., Musie, R. R., Kurniadewi, F., Sukmawati, D., Saamia, V., Wiranatha, M., Abomoelak, B., & Elenshasy, H. A. (2025). Deteksi Vibrio parahaemolyticus Menggunakan Primer Gen toxR2 dengan Gradient Polymerase Chain Reaction. *Jurnal Riset Sains Dan Kimia Terapan*, *11*(1), 19–25. https://doi.org/10.21009/JRSKT.111.03

Ogata, M., Fukamizo, T., & Ohnuma, T. (2021). Thermodynamic Analysis for Binding of 4-O-β-tri-N-acetylchitotriosyl Moranoline, a Transition State Analogue Inhibitor for Hen Egg White Lysozyme. *Frontiers in Molecular Biosciences*, *8*, 654706. https://doi.org/10.3389/fmolb.2021.654706

Otzen, D. (2011). Protein–surfactant interactions: A tale of many states. *Biochimica et Biophysica Acta (BBA) - Proteins and Proteomics*, *1814*(5), 562–591. https://doi.org/10.1016/J.BBAPAP.2011.03.003

Parveen, S., Ali, M. S., Al-Lohedan, H. A., Hoti, N., & Tabassum, S. (2023). Molecular interaction of lysozyme with therapeutic drug azithromycin: Effect of sodium dodecyl sulfate on binding profile. *International Journal of Biological Macromolecules*, *242*, 124844. https://doi.org/10.1016/J.IJBIOMAC.2023.124844

Pasquina-Lemonche, L., Burns, J., Turner, R. D., Kumar, S., Tank, R., Mullin, N., Wilson, J. S., Chakrabarti, B., Bullough, P. A., Foster, S. J., & Hobbs, J. K. (2020). The architecture of the Gram-positive bacterial cell wall. *Nature 2020 582:7811*, *582*(7811), 294–297. https://doi.org/10.1038/s41586-020-2236-6

Pinzi, L., & Rastelli, G. (2019). Molecular Docking: Shifting Paradigms in Drug Discovery. *International Journal of Molecular Sciences 2019, Vol. 20, Page 4331*, *20*(18), 4331. https://doi.org/10.3390/IJMS20184331

Prasetiyo, H., Novita Nanda, F., Rudi, M., & Azila Abdul Razak, N. (2025). Screening of Bioactive Compounds of Spirulina platensis as Potential Antioxidants: An In-silico Approach. *Jurnal Riset Sains Dan Kimia Terapan*, *11*(2), 41–52. https://doi.org/10.21009/JRSKT.112.05

Purwani, D. A., & Kartika, I. R. (2019). PENGARUH VARIASI PENAMBAHAN SUSU SKIM TERHADAP KADAR ASAM AMINO PADA YOGURT SARI KACANG MERAH (Phaseolus vulgaris L.). *Jurnal Riset Sains Dan Kimia Terapan*, *8*(2), 27–36. https://doi.org/10.21009/JRSKT.082.04

Ragland, S. A., & Criss, A. K. (2017). From bacterial killing to immune modulation: Recent insights into the functions of lysozyme. *PLOS Pathogens*, *13*(9), e1006512. https://doi.org/10.1371/JOURNAL.PPAT.1006512

Ramírez, D., & Caballero, J. (2018). Is It Reliable to Take the Molecular Docking Top Scoring Position as the Best Solution without Considering Available Structural Data? *Molecules 2018, Vol. 23, Page 1038*, *23*(5), 1038. https://doi.org/10.3390/MOLECULES23051038

Roy, S., Jana, B., & Bagchi, B. (2012). Dimethyl sulfoxide induced structural transformations and non-monotonic concentration dependence of conformational fluctuation around active site of lysozyme. *Journal of Chemical Physics*, *136*(11). https://doi.org/10.1063/1.3694268

Schrödinger, L. (2021). *PyMOL*. https://www.pymol.org/

Singh, K., Muttathukattil, A. N., Singh, P. C., & Reddy, G. (2022). pH Effect on Ligand Binding to an Enzyme Active Site. *BioRxiv*, 2022.07.01.498456. https://doi.org/10.1101/2022.07.01.498456

Sullivan, M. P., Groessl, M., Meier, S. M., Kingston, R. L., Goldstone, D. C., & Hartinger, C. G. (2017). The metalation of hen egg white lysozyme impacts protein stability as shown by ion mobility mass spectrometry, differential scanning calorimetry, and X-ray crystallography. *Chemical Communications*, *53*(30), 4246–4249. https://doi.org/10.1039/C6CC10150J

Zeng, H. jin, Wang, S. sha, Sun, L. jun, Miao, M., & Yang, R. (2021). Investigation on the effect of three isoflavones on the fibrillation of hen egg-white lysozyme. *Journal of Molecular Recognition*, *34*(6), e2889. https://doi.org/10.1002/JMR.2889